Front. Struct. Civ. Eng. 2022, 16(11): 1453–1473
https://doi.org/10.1007/s11709-022-0877-2

RESEARCH ARTICLE

Effects of microfine aggregate in manufactured sand on bleeding and plastic shrinkage cracking of concrete

Branavan ARULMOLY[a*], Chaminda KONTHESINGHA[a], Anura NANAYAKKARA[b]

[a] *Department of Civil Engineering, University of Sri Jayewardenepura, Mount Lavinia 10370, Sri Lanka*
[b] *Department of Civil Engineering, University of Moratuwa, Moratuwa 10400, Sri Lanka*
[*] *Corresponding author. E-mail: branavanarulmoly@sjp.ac.lk*

ABSTRACT Construction industries have started to utilize manufactured sand (MS) as an effective alternative for river sand in concrete. High-grade parent rocks are crushed to obtain MS, which also produces a considerable amount of microfine aggregate (MFA). The higher percentage of MFA could lead to both positive and negative effects on the performance of cement-based mixes. This research was done to examine the influence of varying MFA levels, specifically 0%, 3%, 6%, 9%, and 12% (by weight) as the partial replacements of MS on bleeding and plastic shrinkage cracking of concrete. In addition to the varying MFA levels, some concrete mixes also included fly ash (FA) and superplasticizer to investigate the effect of free-water content in the mixes. The bleeding test data were taken as on-site measurements, while the cracks from the plastic shrinkage cracking test were evaluated using an image processing technique. The results concluded that the MFA replacements and the effective water-to-cement ratio have a significant effect on the selected concrete properties. With the increasing replacement levels, cumulative bleeding and crack initiation life gradually decreased, while a progressive increase was observed for crack width, crack length, and crack area.

KEYWORDS manufactured sand, fresh concrete, microfines, admixtures, shrinkage, cracking

1 Introduction

Massive projects are underway in the construction industry, which require large quantities of fine aggregates for concrete [1]. Although river sand is considered the most widely used traditional fine aggregate, the over-extraction of river sand near the riverbeds is a serious environmental drawback [2,3]. These days, manufactured sand (MS) is considered an emerging and feasible alternative for river sand in cement-based mixes since river sand is no longer available to fulfill the needs of contractors. MS has both advantages and disadvantages as a fine aggregate due to its physical characteristics [4,5]. Specifically, the cubical shape and rough surface texture of MS particles could significantly increase the bonding strength characteristics due to the particle interlocking behaviour [6,7]. These properties play a vital role in the production of special concretes, such as high-strength and ultra-high strength concretes [8–10]. On the other hand, the fresh state properties of cement-based mixes, in particular the workability and consistency, are affected by the resistance to free-flow of fresh mixes and the low lubricating effect between the cement paste and aggregates [11,12].

MS is a fine aggregate purposely made by crushing high-grade parent rocks through several crushers to obtain the required particle size distribution. This process enables certain special physical characteristics, as discussed above, as well as different ingredient compositions of MS. Microfine aggregate (MFA) is the most crucial ingredient of MS that highly influences the performance of both fluid and hardened concrete. Several studies [1,13–17] suggested that the functionality of hardened concrete improves when a considerable amount of MFA is present in MS. He et al. [1], Li et al. [13], and Wang et al. [14] reported the highest compressive strength, flexural strength, freeze−thaw durability and the lowest water and chloride ion permeability of concrete

Article history: Received Mar 12, 2022; Accepted Jun 5, 2022

when MS contained 10% of MFA. Stewart et al. [16] revealed that the compressive and flexural strengths of concrete were improved with 13% of stone powder content.

Several negative outcomes were also reported for higher MFA contents. Gotmare and Sheth [17] revealed that the higher MFA content increased water demand, which caused a reduction in strength and an increase in drying shrinkage of concrete. Arulmoly et al. [7] evinced higher capillary water absorption for MS mortars compared to river sand mortars due to an increase in the total specific surface as a result of considerable MFA content. Furthermore, a marginal increase in the initial and final water absorptions was observed for 6% limestone powder (by weight) added concrete than the control roller compacted concrete pavement mix in the study conducted by Hashemi et al. [18].

Bleeding and plastic shrinkage cracking are essential properties of plastic stage concrete. Plastic shrinkage cracking mainly occurs in concrete elements that are larger in surface area and smaller in depth. The principal phenomenon behind plastic shrinkage cracking is the rapid evaporation of accumulated water as a result of bleeding [19]. Bleeding usually takes place when aggregate particles settle due to gravity, which enables an upward movement of water towards the surface through the particle pores [19,20]. Climate conditions, such as excessive heat and wind, may also accelerate the rate of water evaporation on the concrete surfaces. The cracking of concrete begins when tensile pressure is created after the complete evaporation of bled water from the surface [20–22]. This negative pressure pulls back the particles, causing the formation and propagation of shrinkage cracks and, ultimately, the failure of concrete.

Several proposed factors influence the bleeding and plastic shrinkage cracking of concrete. A concise review of literature shows that a considerable number of studies investigated the effects of varying cement properties [23–25], addition of fibres [26–29], and inclusion of shrinkage reducing admixtures [30,31] on concrete bleeding and plastic induced cracking. However, another important factor is the presence of MFA in MS, which has not appeared in any published literature to date. This could be imperative when concrete is prepared with MS alone as it generally contains a considerable amount of MFA. The underlying rationale is that the particle size of MFA is generally less than 0.075 mm, making the particles lightweight with a very low specific gravity compared to other aggregate particles [27]. When a fresh concrete mix enters a steady state following mixing, the coarser particles settle down and bleeding begins to form at the top surface of concrete. However, low settlement rate of MFA particles due to a large variation in specific gravities could significantly reduce the settlement rate of the coarser particles. This could, in turn, significantly affect the bleeding rate and vulnerability to plastic shrinkage cracking of concrete.

On the other hand, water demand may be also affected by the presence of MFA due to its fineness. The finer MFA fraction could lead to a larger specific surface area of aggregates that requires more water to achieve the design slump [32,33], which could result in more concrete bleeding. Several studies demonstrated the effects of water-to-cement ratio or water demand of the mix on the plastic shrinkage cracking of concrete [34,35]. These studies concluded that the rate of concrete bleeding is directly related to the amount of water present in the mix. Furthermore, the types and dosages of water reducing admixtures may also impact the free-water content of concrete, which may lead to variations in bleeding and plastic shrinkage cracking.

Plastic shrinkage cracking is a salient failure of plastic concrete that determines its long-term performance. The corrosion of reinforcement is exacerbated when the corrosion accelerators penetrate through the shrinkage cracks. However, it should be noted that other factors, such as concrete ingredients (cement paste and aggregates) and interfacial transition zone (ITZ) may also determine concrete durability. The ITZ has high porosity and should be efficiently treated to reduce the corrosion of concrete. This could be achieved by certain enhancing surface treatment process of aggregates. Sun et al. [36] conducted a similar study investigating the corrosion resistance of concrete exposed to a chloride-induced environment when aggregates are coated with slag and silica fume. The authors identified that the inclusion of both slag and silica fume reduced the porosity of ITZ, with silica fume reducing more than 40% of porosity. Another brief study was executed by Sun et al. [37] on the reliability-based numerical model for assessing the corrosion of concrete subjected to a sulfate-induced environment. A time-dependent reliability index was predicted with consideration for the uncertainties of cement chemical composition and ITZ porosity under chronic sulfate attack. The authors identified that the time taken to prepare concrete with silica fume-coated aggregates was significantly shortened to reach the reliability index limit with increasing sulfate concentration.

Both crack development and the effect of cracking on the corrosion of reinforcement are time-dependent processes. Based on the study implemented by Chen et al. [38], it is clear that the corrosion of reinforcement continues over time even if the surface crack is repaired through periodic maintenance. One of the factors that determines the continuous corrosion of reinforcement may be the composition of concrete. Hence, the materials for concrete preparation should be carefully selected and properly treated prior to application.

2 Research significance

The higher presence of MFA in MS leads to several threats to both fresh and hardened concrete, as well as the long-term performance of concrete. BS 882 [39] set the maximum allowable limit of MFA (i.e., particles less than 0.075 mm) in MS as 16% for concrete usage. However, lack of conviction remains whether this allowable value can be further applied to concrete as high MFA content leads to serious drawbacks in strength and water demand of the mixes. Several studies showed different optimum permissible percentages of MFA in terms of the properties of hardened concrete. Due to the scarcity of available information regarding the fresh properties of concrete, this study aimed to investigate the allowable optimum MFA in MS concrete by inspecting concrete bleeding and plastic shrinkage induced cracking. In this study, the maximum permissible MFA content is evaluated in regards to the rate of bleeding, cumulative bleeding, and plastic shrinkage crack properties, such as crack initiation life, crack width, crack length, and crack area, which is a novel concept. In addition, the combined influence of varying MFA levels in MS and water reducing capacity of mineral and chemical admixtures on bleeding and plastic shrinkage cracking is also examined, which has not been reported in any literature.

3 Experimental setup

3.1 Materials

3.1.1 Cement

An Ordinary Portland Cement (OPC) classified under the 'CEM I 42.5N' of BS EN 197-1 [40] was used as the binding agent for each concrete. The properties of OPC, according to the technical specifications, are listed in Table 1, with each property verified against the limitations given in the above standard. The chemical properties of OPC are mentioned in Table 2.

3.1.2 Manufactured sand

In the present study, MS is included in the concrete mixes as the fine aggregate. Two types of MS, specifically MH and MC, were selected based on the production sources. MH (see Fig. 1(a)) defines the MS produced from Hornblende-Gneiss rock and MC (see Fig. 1(b)) is denoted by the MS produced from Charnockite rock. The particle size distribution of both MS types is illustrated in Fig. 2. Based on the gradation curves, we can see that the percentage of particles greater than 1.16 mm and less than 4.75 mm of MH and MC were slightly higher than the allowable limitations defined in ASTM C33 [41]. Furthermore, the percentage of particles greater than 0.075 mm and less than 0.2 mm also marginally exceeded the required region. The reason for this could be the dependence of MS gradation on the crushing stages during production, where varying equipment efficiencies could differ the degree of particle sizes [42]. However, the present study will not address on this concept, but rather focus on the influence of MFA levels.

The chemical compositions of various MS types were obtained through X-ray fluorescence technique and Table 2 provides the compositions detected from the experiment. Since the SiO_2 content was greater than 70%, the sources selected for both MS types shall be classified as 'silicate rocks', which work well with the performance of cement-based mixes and highlights the durability of the selected MS types in concrete. Moreover, X-ray diffraction test was carried out on the powdered samples of Hornblende-Gneiss and Charnockite rocks. Table 3 shows the minerals identified in those sources. The potentially detrimental minerals for the performance of concrete suggested by ASTM C294 [43], such as illite and biotite were identified in very low quantities. Generally, illite and biotite could lead to serious issues in the long-term performance of concrete. Illite coats the aggregates and reduces their bonding capacity with the cement paste. Biotite increases the water demand of the mixes due to its flaky and elongated surfaces, reducing the overall strength of concrete. Because of the scarcity of these harmful minerals, a risk-free application of the selected MS types in concrete shall be assured.

Table 4 lists the physical properties relevant to the

Table 1 Properties of OPC

property	selected cement	EN 197-1 [40] limits
compressive strength (2 d) (N/mm^2)	> 25	⩾ 10
compressive strength (28 d) (N/mm^2)	> 52	42.5–62.5
setting time (min)	130–150	⩾ 60
fineness (m^2/kg)	330–340	not defined
soundness (mm)	< 1	⩽ 10
relative density	~ 3.08	not defined
chloride content	< 0.08%	⩽ 0.1%
insoluble residue (IR)	< 3.0%	< 5.0%

Table 2 Chemical and mineralogical compositions of concrete ingredients (wt.%)

material	SiO_2	Al_2O_3	Fe_2O_3	CaO	MgO	SO_3	Na_2O	K_2O	LOI
MC	72.01	7.83	2.09	3.95	0.25	0.00	2.08	2.54	–
MH	73.59	7.59	4.83	3.07	1.02	0.00	1.75	1.33	–
FA*	63.47	26.22	5.27	0.71	0.33	0.28	0.018	0.039	2.55
OPC*	22.58	2.54	0.64	59.24	2.61	2.48	–	–	2.89

*Note: Data provided in the technical specifications. LOI: Loss on ignition.

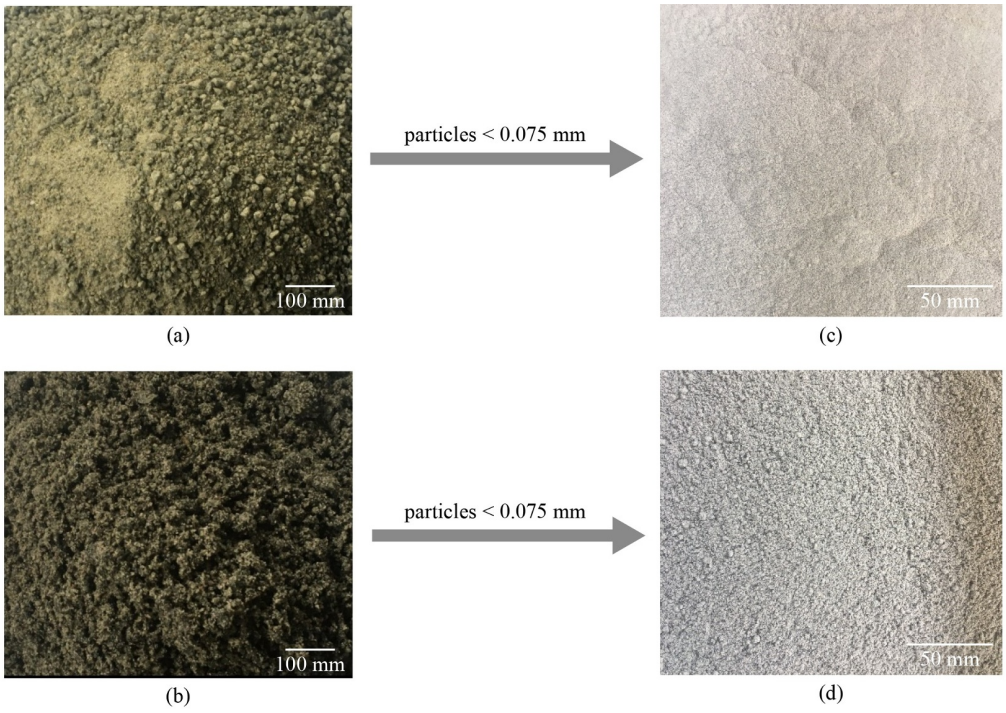

Fig. 1 MS and MFA types: (a) MC; (b) MH; (c) MFA-MC; (d) MFA-MH.

concrete mix design and experiments conducted in this study. The corresponding standards for the determination of each property are also included. Based on the fineness modulus and specific gravity, it can be observed that MH is slightly coarser and heavier than MC. Both MS types demonstrated similar loose densities, though the packing density of MH is considerably higher than that of MC. This could be due to the increased MFA content of MH (6.28%) compared to MC (3.37%) since the micropores between the coarser sand particles could be filled with this increased fine particle content. Small quantities of silt were also present in both types. No chloride or salt, two main accelerators of corrosion of reinforcement, was detected in the selected MS types. Therefore, these MS types could be applied in reinforced concrete to ensure long-term performance.

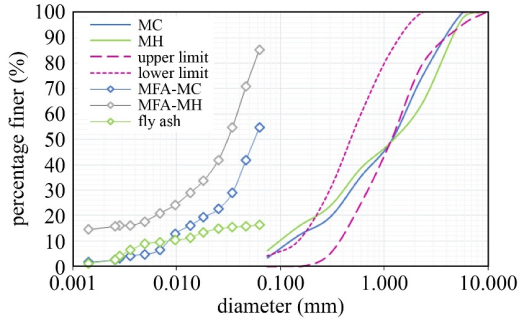

Fig. 2 Particle size distribution of MS types, MFA types, and FA.

Table 3 Mineralogical compositions of the sources for MC and MH (wt.%)

material	calcite	quartz	albite	k-feldspar	anorthite	dolomite	illite	biotite
MC	18.97	27.95	18.03	27.15	4.36	0.23	1.66	0.00
MH	0.62	49.48	10.44	10.68	20.30	0.22	6.23	0.02

3.1.3 Microfine aggregate

The influencing parameter of the present study is the percentage of MFA added to concrete. Here, MFA that complies with BE 882 [39] is defined as MS particles that can pass through the 0.075 mm sieve. Initially, the required amount of MFA was prepared in the laboratory using a wet sieving method as described in ASTM C117 [49]. The sieved contents were then oven-dried

Table 4 Physical properties and deleterious contents of MC and MH

material	fineness modulus ASTM C144 [44]	specific gravity ASTM C128 [45]	loose density (kg/m^3) ASTM C1252 [46]	packing density (kg/m^3) ASTM C29 [47]	water absorption (%) ASTM C70 [48]	deleterious contents (%)	
						MFA ASTM C117 [49]	silt
MC	3.086	2.70	1740	1824	1.1	3.37	1.92
MH	3.107	2.71	1784	1915	1.2	6.28	2.88

continuously for 48 h and stored in air-tight containers. Figures 1(c) and 1(d) show the MFA obtained from the selected MS types, where MFA-MC represents the MFA obtained from MC and MFA-MH represents the MFA obtained from MH. Furthermore, the particle size distributions of both MFA types were investigated using a hydrometer analysis test based on ASTM D7928 [50]. The gradation curves of MFA-MC and MFA-MH are presented in Fig. 2.

MFA is a by-product from aggregate crushing plants, which are the dust-of-fracture of high-grade metamorphic rocks. Therefore, MFA is also known as 'mineral fines' (i.e., the crushed form of minerals presents in the parent rocks). Generally, the reaction rate of aggregates is influenced by its fineness since higher fineness causes higher reaction rates with other chemical compositions. Here, the dust nature of MFA could lead to both advantages and disadvantages in the mechanical and durability characteristics of concrete. The performance of MFA should be carefully investigated due to the possibility of it containing reactive harmful minerals. For example, the reactive form of mica lowers the strength of concrete due to the improper adhesion between the cement paste and the flat and smooth surface of the mica particles [51,52]. The durability of concrete may also be deteriorated if water and air accumulate beneath the flaky mica particles. The presence of mica may also have serious effects on the freeze−thaw expansion and contraction response of concrete [53]. Fortunately, the mica content in the parent rock sources selected in this study are negligible, which reduces the issues mentioned above.

3.1.4 Admixtures

The main purpose of using admixtures is to reduce the water demand for concrete mixes and investigate the selected concrete properties with the available water content. Both mineral and chemical admixtures were selected for this study since they may reduce the water demand to various extents. Fly ash (FA) and superplasticizer (SP) were utilized as the mineral and chemical admixtures, respectively. In order to avoid the variations in admixture content, the dosages of FA and SP were maintained at 15% and 1.2% (by OPC mass), respectively. According to the technical requirements stated in ASTM C618 [54] and ASTM C494 [55], the selected FA was classified as 'Class F fly ash', while the selected SP was categorized as 'polycarboxylate and modified phosphonate superplasticizer—Type A and F'.

3.2 Batching of materials and concrete mix design

Materials for concrete were acquired on a weight basis. Prior to batching, all materials were stored at a temperature of (28 ± 4) °C, which also remained constant throughout the mixing of concrete. To study the effects of varying MFA levels, MC and MH were partially replaced by its own MFA (i.e., by MFA-MC and MFA-MH, respectively). The weight of MS in concrete was replaced at 0%, 3%, 6%, 9%, and 12% by MFA. The concrete with 0% MFA was used as the control mix to compare the performances of other concrete mixes.

For the concrete designed with lower MFA levels, such as 0% or 3%, the MC and MH were first sieved with a 0.075 mm sieve to completely remove the initial MFA that make the MFA content higher than 3%. Then, the required MFA was measured from the stored contents using an electronic balance and mixed with the sieved MC and MH. For the other replacement levels, such as 6%, 9%, and 12%, the required MC and MH were measured without sieving and the additional required MFA was blended with the unsieved MC and MH. In all cases, the total fine aggregate content (i.e., the summation of MS and MFA) was checked to make sure accurate quantities of the required materials were obtained using the mix design calculations.

The mix design of concrete was done based on the saturated surface dry (SSD) condition of aggregates. At the preliminary stage, it is required to identify the moisture content of the selected MS types at the SSD condition using a standard method described in BS 812-2 [56]. Several attempts were used to achieve the required free-running condition of MC and MH suggested by the standard. Figure 3 presents the free-running shape of MC and MH obtained during SSD condition. Afterwards, the

(a) (b)

Fig. 3 Free-running shape at SSD condition: (a) MC; (b) MH.

representative MC and MH samples were oven-dried at (100 ± 5) °C for at least 24 h to determine the moisture contents at SSD condition.

Each concrete was designed with a grade of M30. The initial water-to-cement ratio $(w/c)_i$ was set as 0.5 and the mixes were designed for a slump of (110 ± 10) mm. The mixing of concrete was carried out using a mini concrete mixer with a capacity of 0.2 m^3 and the total mixing time was maintained at (10 ± 5) min for each mix. The OPC and MS were first thoroughly mixed before MFA was added. After that, coarse aggregate was introduced into the mixer. For M-series concrete mixes, FA was added and then water was gradually added until the pre-defined slump was achieved. SP was mixed normally with a portion of the total measured water and then added to the mix.

For the pre-defined design slump to maintain constant throughout the study, the workability of each concrete was regularly checked during mixing through slump trials as per ASTM C143 [57]. This method allowed us to check whether the design slump has been achieved or if additional water is required. For example, if a mix did not achieve the design slump, it was re-mixed with the addition of water to increase the slump. This process was repeated until the mix reached the design slump. Once the concrete attained the required slump, the actual *w*/*c* ratio was determined as the effective *w*/*c* $(w/c)_{ef}$ based on the total water content in the mix. Here, the total water content is the summation of the initial water calculated from the mix design and the additional water introduced to the mix to achieve the design slump. All concrete mixes were categorized into three series: P series, M series, and C series, which define the plain concrete (i.e., concrete without any admixtures), concrete with FA, and concrete with SP, respectively. Table 5 tabulates the mix proportions of the constituents for each concrete series.

3.3 Experiments

3.3.1 Bleeding

The bleeding test was carried out according to the standard procedures under 'Method A' of ASTM C232 [58]. This procedure is based on the consolidation of fresh concrete using a rodding method without any external vibrations. A cylindrical steel container with a 250 mm diameter, 280 mm inside height, and an approximate 3 mm thickness was filled with concrete immediately after the mix reached the required slump. The total time for introducing fresh concrete into the bleeding container was maintained at (5 ± 2) min to minimize the effects of slump reduction. The experimental setup used for the bleeding test is shown in Fig. 4(a).

A straight steel tamping rod with a 16 mm diameter and hemispherical tip was used for the rodding compaction of concrete. The filling and surface finishing of concrete was done up to a height of 250 mm from the bottom of the container to enhance the extraction of accumulated bleed water. Following filling and compaction, the container was covered with a lid to prevent any evaporation of the bled water.

The container and its contents were carefully placed on a level platform without any vibrations and exposed to the same environmental conditions for the plastic shrinkage cracking test. The accumulated bleed water was drawn off using a syringe at 10-min intervals during the first 40 min and at 30-min intervals afterwards until 160 min (the average time for ceasing bleeding from the trial experiments). At each extraction, the bled water was transferred into a 100 mL glass measuring cylinder with an air-tight lid and the cumulative weight was measured using an electronic balance sensitive to 0.1 g. Two test samples were prepared to determine the bleeding for each mix. The two results were averaged to obtain the final results.

3.3.2 Plastic shrinkage cracking

The susceptibility of concrete for plastic shrinkage induced cracking was investigated inside a climate chamber to maintain stable environmental conditions throughout the experiment. A rectangular mould with the internal dimensions of 560 mm × 355 mm × 100 mm was fabricated with a stress riser (i.e., which acts as the crack inducer) at the middle that complies with the standard ASTM C1579 [59]. Two metal inserts were provided next to the stress riser to accommodate the internal restraints of concrete during shrinkage. However, several previous studies reported that the provision of only two metal inserts next to the stress riser was not sufficient to restraint the concrete during hardening. Therefore, the specimen prepared according to ASTM C1579 [59] was further modified in this study using six additional 10 mm diameter corrosion-free end bolts and nuts at both shorter spans of the mould as shown in Figs. 4(b) and 4(c).

For the provision of nuts and bolts, the shorter spans were selected because concrete generally shrinks quicker from the edges along its longer span. Here, it should be noted that the nuts were kept at the edges of bolts, which could efficiently restraint the concrete without shortening from the edges of the mould. With these modifications, large cracks were visible along the stress riser provided at the middle of the specimen. These modifications were also used in the studies conducted by Sayahi [60] and Sivakumar and Santhanam [61] with minor deviations.

Once the defined slump was attained, the concrete mix was introduced into the plastic shrinkage cracking mould a layer at a time to reduce the effects of compaction on bleeding. After the mould was filled entirely with

Table 5 Mix proportions of concrete ingredients

series	mix code	main constituents of concrete (kg/m^3)				$(w/c)_i$	contribution of supplementary materials (%)			
		OPC	MC	MH	CA		MFA-MC	MFA-MH	FA	SP
P	P-MC$_0$	450	799	–	903	0.5	0	–	–	–
	P-MC$_3$	450	775	–	903	–	3	–	–	–
	P-MC$_6$	450	751	–	903	–	6	–	–	–
	P-MC$_9$	450	727	–	903	–	9	–	–	–
	P-MC$_{12}$	450	703	–	903	–	12	–	–	–
	P-MH$_0$	450	–	765	937	–	–	0	–	–
	P-MH$_3$	450	–	742	937	–	–	3	–	–
	P-MH$_6$	450	–	719	937	–	–	6	–	–
	P-MH$_9$	450	–	696	937	–	–	9	–	–
	P-MH$_{12}$	450	–	673	937	–	–	12	–	–
M	M-MC$_0$	396	799	–	903	0.5	0	–	15	–
	M-MC$_3$	396	775	–	903	–	3	–	15	–
	M-MC$_6$	396	751	–	903	–	6	–	15	–
	M-MC$_9$	396	727	–	903	–	9	–	15	–
	M-MC$_{12}$	396	703	–	903	–	12	–	15	–
	M-MH$_0$	396	–	765	937	–	–	0	15	–
	M-MH$_3$	396	–	742	937	–	–	3	15	–
	M-MH$_6$	396	–	719	937	–	–	6	15	–
	M-MH$_9$	396	–	696	937	–	–	9	15	–
	M-MH$_{12}$	396	–	673	937	–	–	12	15	–
C	C-MC$_0$	445	799	–	903	0.5	0	–	–	1.2
	C-MC$_3$	445	775	–	903	–	3	–	–	1.2
	C-MC$_6$	445	751	–	903	–	6	–	–	1.2
	C-MC$_9$	445	727	–	903	–	9	–	–	1.2
	C-MC$_{12}$	445	703	–	903	–	12	–	–	1.2
	C-MH$_0$	445	–	765	937	–	–	0	–	1.2
	C-MH$_3$	445	–	742	937	–	–	3	–	1.2
	C-MH$_6$	445	–	719	937	–	–	6	–	1.2
	C-MH$_9$	445	–	696	937	–	–	9	–	1.2
	C-MH$_{12}$	445	–	673	937	–	–	12	–	1.2

concrete, the sides were tamped by a steel rod until the concrete was approximately level at the top. At the end of screeding, the concrete was leveled with a trowel and, immediately, the mould and its contents were placed inside the climate chamber. Figure 5 presents the experimental setup used for the plastic shrinkage determination. One test specimen was prepared for this for each concrete mix. It was also ensured that the bleeding and plastic shrinkage cracking setups were susceptible to the designed environmental conditions simultaneously.

To satisfy the minimum requirements for plastic shrinkage cracking mentioned in ASTM C1579 [59], the climate chamber was maintained at a constant temperature of (40 ± 5) °C, relative humidity of 20% ± 5%, and wind speed of (10 ± 1) m/s. Most of the concrete mixes showed an initial temperature range of (25 ± 2) °C. Hence, the average evaporation rate inside the climate chamber was determined as (1.5–2) kg·m^{-2}·h^{-1} from the 'evaporation nomograph' proposed by Kosmatka et al. [32].

3.3.3 Crack investigation and interpretation

The concrete specimens for plastic shrinkage cracking were continuously inspected to identify crack initiation. A high intensity discharge lamp was not only used as the

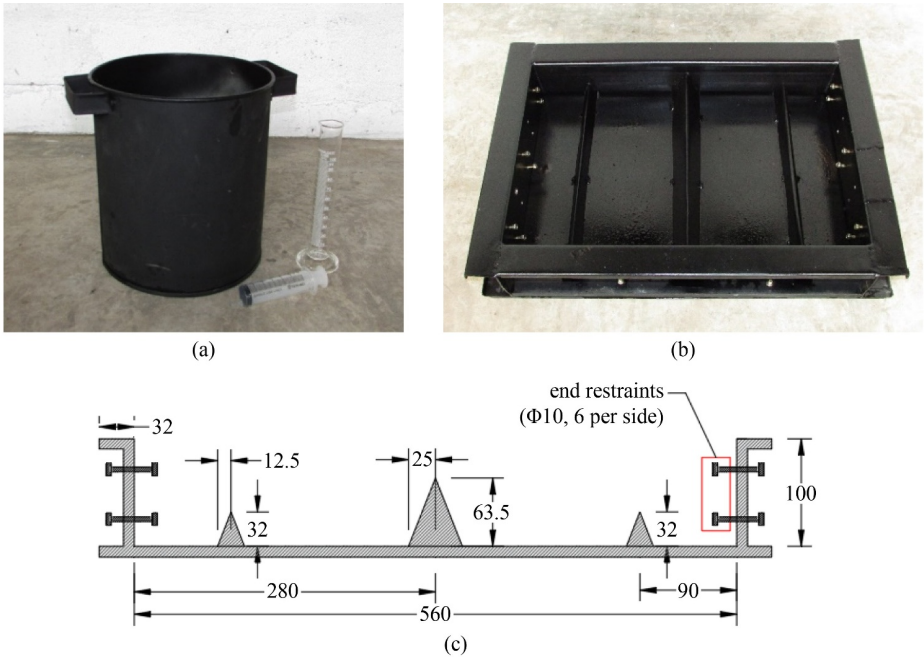

Fig. 4 Experimental setups: (a) bleeding test setup; (b) plastic shrinkage cracking device; (c) arrangement of plastic shrinkage cracking device (all dimensions are in mm).

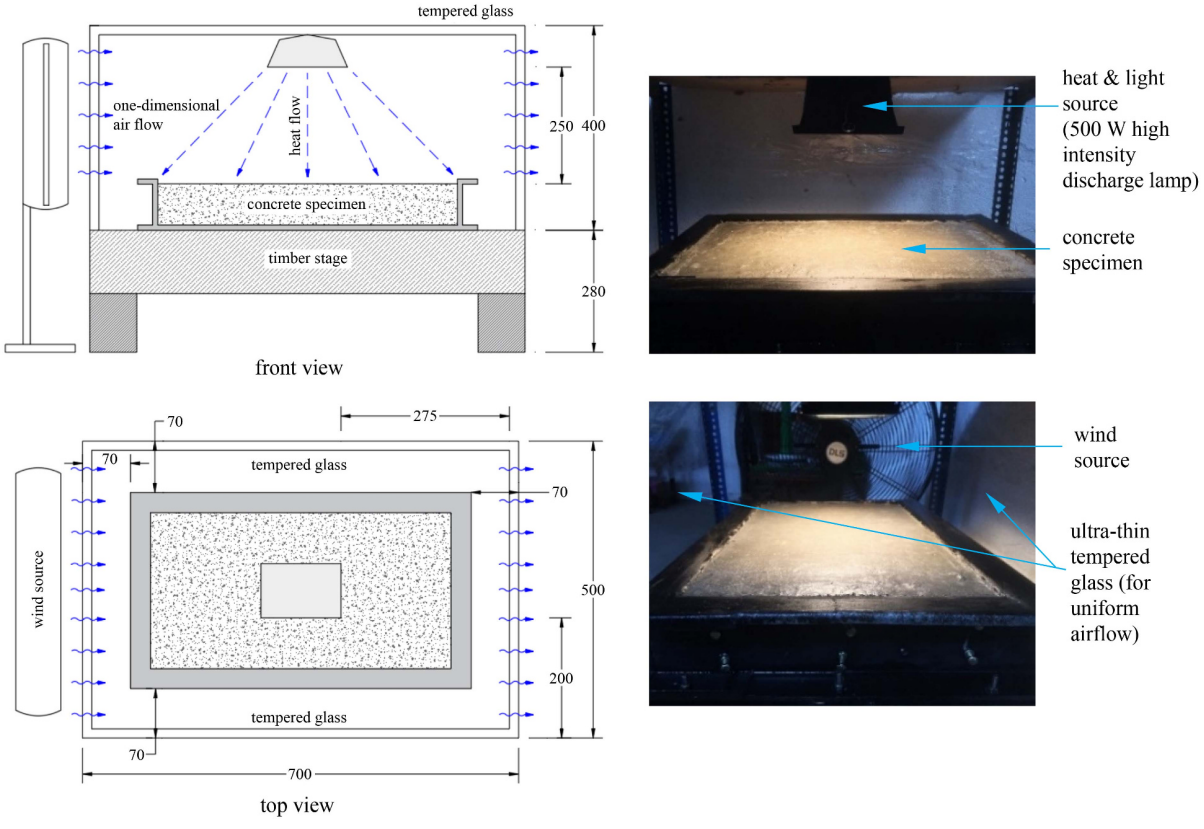

Fig. 5 Plastic shrinkage cracking test setup (all dimensions are in mm) (Arulmoly et al. [62]). (Reprinted from Structural Concrete, Arulmoly B, Konthesingha C, Nanayakkara A, Plastic settlement and hardened state assessments of manufactured sand made concrete for varying microfine levels, 1–21, Copyright 2022, with permission from John Wiley and Sons.)

heat source, but also as the light source that aided in the visual inspections during light-time. The 'crack initiation life' was recorded as the duration between the first exposure of the concrete specimen to the climate

conditions and first observation of hairline cracks at the surface.

The crack measurements and investigations began after the concrete specimens were exposed to the climate conditions for at least (24 ± 2) h to ensure full development and stabilization of cracks initiated at the surface. After the required period, the developed cracks were photographed using a 16× Digital Single-Lens Reflex camera with a measuring scale on the surface of concrete specimen to scale images for processing.

The crack detection, characterization, and measurements were executed using an image processing technique and the 'ImageJ' software. Before implementing the crack detection model, as described in Fig. 6, the raw images were calibrated by setting a scale for the assigned known length using the software. The first stage after calibration was gray scaling and enhancing by setting the images to an 8-bit grayscale type. The grayscale images were then cleaned, filtered, and binarized to reduce the background noise and subsequently enhanced for better crack detection. After that, image thresholding was set at 72.5% for better crack illumination. The illuminated cracks were then detected using crack boundaries and edges using a similar methodology as that found in the research done by Qi et al. [63] and Turkmenoglu et al. [64].

Once the crack contour was detected, further image processing was done to analyze the cracks. The profile of the crack was clearly defined using the illuminated boundaries and outlines as presented in Fig. 7. Prior to

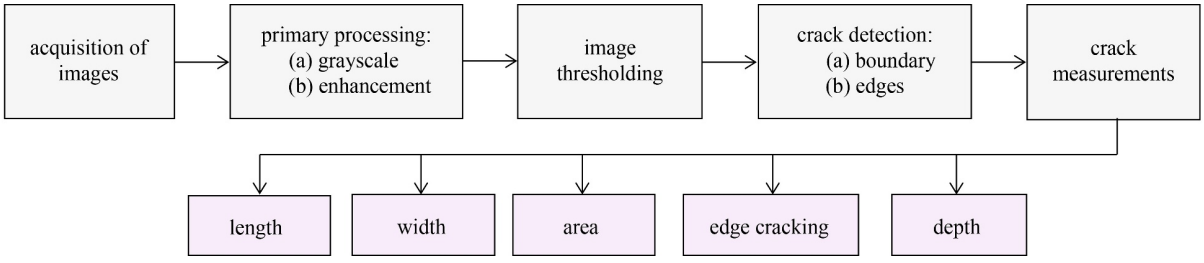

Fig. 6 Crack detection model based on image processing technique.

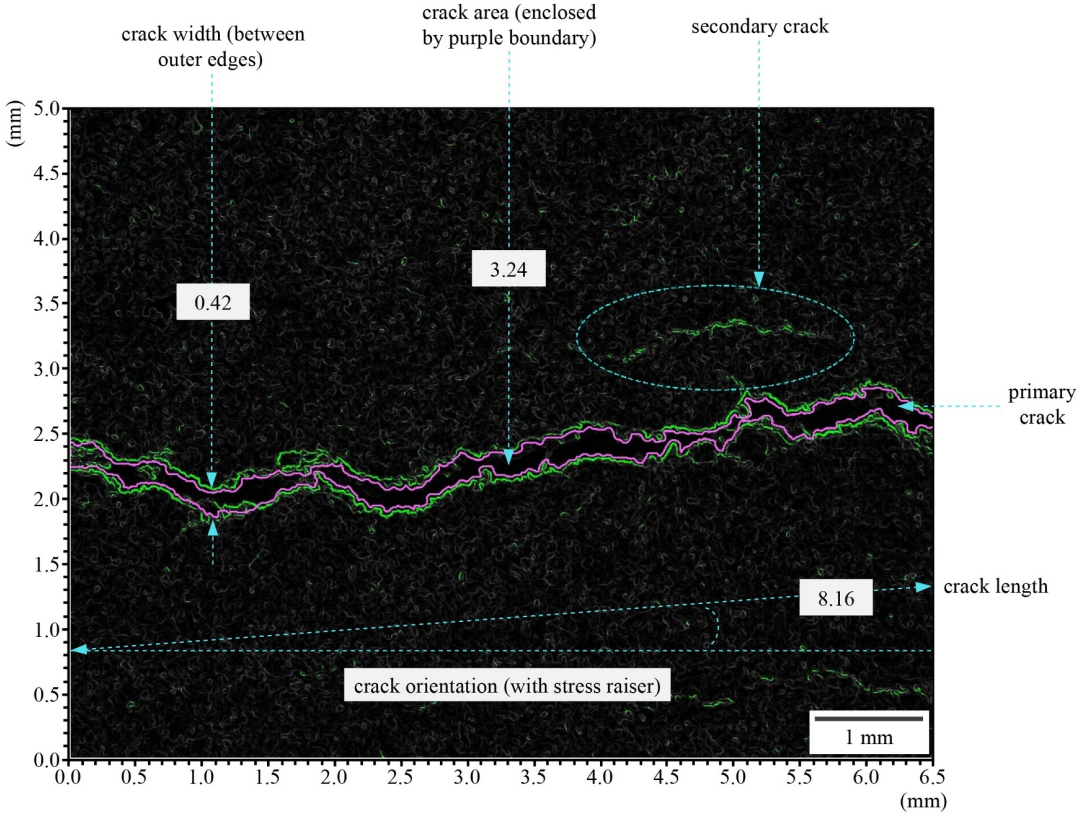

Fig. 7 Measurements of a primary crack (boundary detected threshold image) (Arulmoly et al. [62]). (Reprinted from Structural Concrete, Arulmoly B, Konthesingha C, Nanayakkara A, Plastic settlement and hardened state assessments of manufactured sand made concrete for varying microfine levels, 1–21, Copyright 2022, with permission from John Wiley and Sons.)

crack measurements, the crack profiles were categorized based on the crack patterns. It was observed that the cracks propagated along the stress riser, thus the crack lengths were measured using a line of best fit. For segmented cracks, the total length was determined by adding the lengths of each segment.

The width of the crack was quantified perpendicular to the stress riser at 20 mm intervals along the longitudinal profile starting from one edge of the crack to the other. The width was measured between the two outer perimeters of the crack boundary, and the average crack width and maximum crack width were determined. Crack area quantification of many previous studies were conducted based on the total length and average width of cracks [65,66]. However, the accuracy of this area calculation may not be sufficient due to the large variations in crack widths and curvatures. Therefore, the 'Polygon sections' software tool was used to estimate the crack area. Furthermore, the depth of the cracks was evaluated by observing the side views of the hardened specimens after their removal from the device. The crack depths were measured at the longer spans of the specimen near the stress riser and used to calculate the average depth.

3.4 Statistical analysis

To visually inspect the significance of replacing MS with MFA, the concrete properties were plotted against the replacement levels of MFA. Vertical error bars were provided for each replacement level at the standard 95% confidence interval and the significance was identified based on the interception of error bars.

In addition, a standard single factor one-way analysis of variance (Table 7) test was performed to determine the statistical significance of varying the MFA content on the bleeding and plastic shrinkage cracking of concrete. Here, five independent groups were decided according to the replacement levels of MS by MFA, specifically 0%, 3%, 6%, 9%, and 12%. The level of statistical significance was evaluated between these five groups. The null hypothesis was 'no significant effect of the replacement of MS with MFA on the property of concrete' and this was checked at 95% confidence interval ($\alpha = 0.05$).

4 Results and discussion

4.1 Effect of MFA on bleeding

Figure 8 shows the bleeding of the P-series concrete by time for each replacement level. It was observed that as the replacement levels of MS by MFA increased, the bleeding of concrete decreased (i.e., curves moved from top to bottom as the replacement levels increased from 0% to 12%). The rationale behind the reduced bleeding at higher MFA contents could be due to the replacement of the coarser aggregate particles by MFA, a finer aggregate, resulting in a lower particle settlement. A similar behaviour was seen in the study conducted by Ghourchian et al. [23] on the effects of fineness in different cement types. It should be noted that a drastic decline was observed when the MFA replacing level increased from 3% to 6%, as seen in Fig. 8(a). Though the exact reason for this is unknown, it may be due to the optimum settling behaviour of coarser particles when the MFA content was 0% and 3%. A future study on this behaviour is necessary to better understand the drop observed between these curves.

Results also showed that as the MFA content in P-series concrete increased from 0% to 12%, the water remaining after the design slump was reduced from 0.263 to 0.209 kg/m^3 for MC concrete and from 0.241 to 0.205 kg/m^3 for MH concrete. For RS concrete, the excess water was 0.302 kg/m^3. This reflects how the higher replacement levels of MS by MFA could increase the total specific surface area of aggregates, increasing the water content required to achieve the pre-defined slump, as well as the water retained in the mix.

Furthermore, the MC and MH concretes showed a

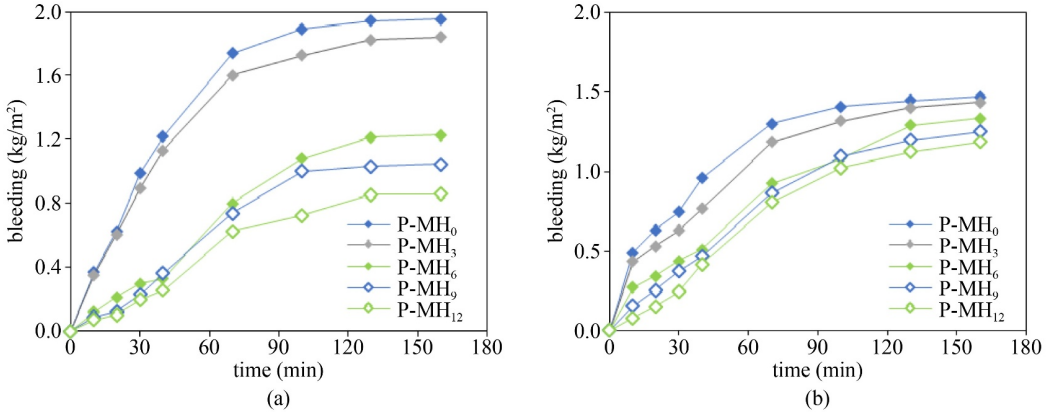

Fig. 8 Variation of bleeding of P-series concrete with time: (a) MH concrete; (b) MC concrete.

gradual increase at the beginning for each MFA level, which slowed down from 90 to 120 minutes. This behaviour was influenced by the amount of water available in the mix required for stiffening. Bleeding was halted when concrete reached the initial setting [19,22]. At 160 minutes, it was observed that the coarser MH considerably increased the cumulative bleeding of concrete compared to MC due to its quicker particle settlement A similar behaviour was also observed in Figs. 9 and 10 for the M- and C-series concrete, respectively.

The addition of FA decreased the rate of bleeding of M-series concrete than P-series concrete at each replacement level. According to Fig. 9, the optimum bleeding attained by the M-series concrete with MH and MC were 1.37 to 1.63 kg/m^2 and 1.32 to 1.51 kg/m^2, respectively. These were considerably less than the ranges 0.85 to 1.95 kg/m^2 and 1.18 to 1.47 kg/m^2, which were obtained from the P-series concrete with MH and MC, respectively. It can be determined that the rate of bleeding up to 90 minutes was similar for each M-series concrete mix, which was not the case for the P-series. Hence, it can be concluded that the initial rate of bleeding was mainly influenced by the inclusion of FA rather than the MFA replacement levels.

Here, FA was used as a cementitious material, which is finer than OPC. Therefore, the effective fineness was increased due to the partial replacement of OPC by FA, which resulted in the slightly reduced bleeding of concrete. Here, it should be noted that the addition of FA was maintained at 15% for each M-series concrete mix. The addition of 15% FA by replacing cement reduced the water required for the M-series concrete mixes to achieve the design slump to 5%–6.2%. Therefore, the actual water content in the M-series concrete mixes was lower compared to the P-series, which resulted in the lower bleeding.

As seen in Fig. 10, two bases for the bleeding rate trends of the C-series concrete shall be concluded. Due to the scarcity of mineral admixtures, variations in the mixes' fineness were solely due to the varying MFA contents. The optimum bleeding was achieved from 0.79 to 0.91 kg/m^2 and 0.60 to 0.84 kg/m^2 when MH and MC were respectively replaced by MFA from 12% to 0%. The optimum bleeding levels were approximately 40% to 50% lower than that of the P-series concrete. The high range water reducing SP that was used played a pivotal role in the declination of bleeding. It was identified that the inclusion of 1.2% SP minimized the water requirement to 11.5% to 14% compared to the plain

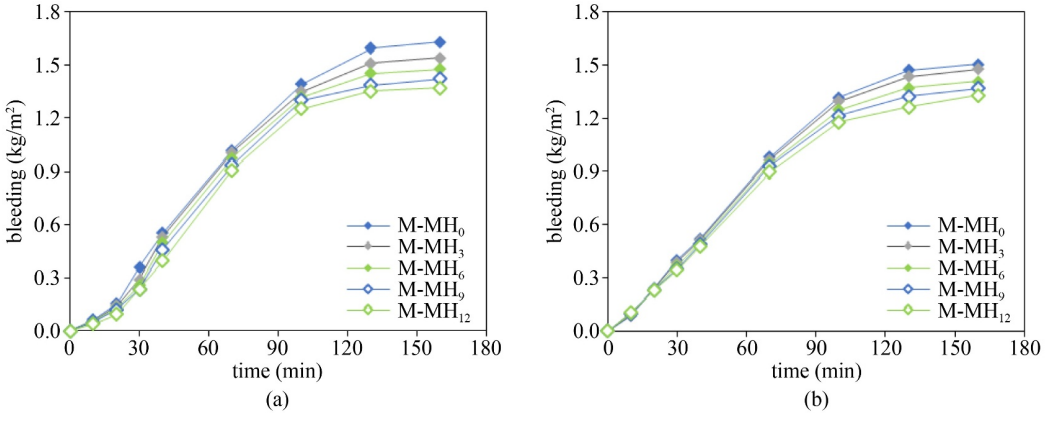

Fig. 9 Variation of bleeding of M-series concrete with time: (a) MH concrete; (b) MC concrete.

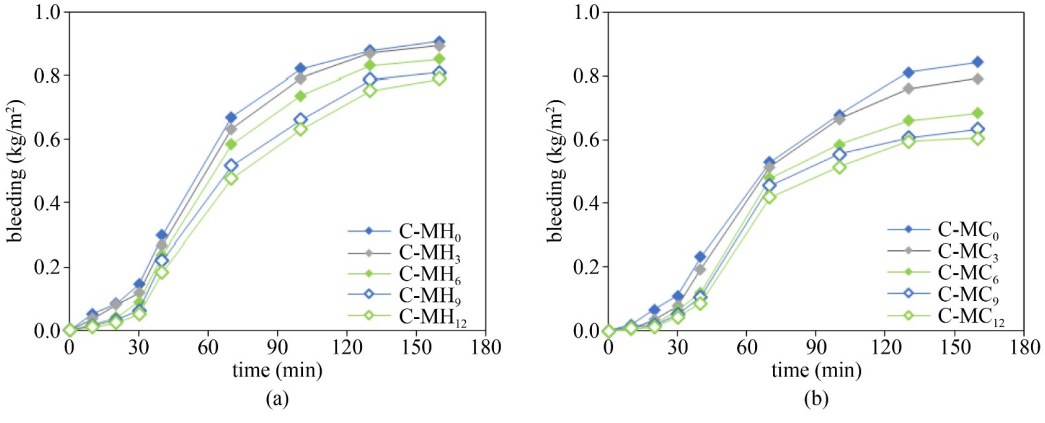

Fig. 10 Variation of bleeding of C-series concrete with time: (a) MH concrete; (b) MC concrete.

concrete. This is a significant reduction in the amount of free-water in the mixes, which resulted in considerably lower bleeding in the C-series concrete than P-series and M-series concretes.

As seen in Fig. 11, the cumulative bleeding of each concrete series gradually decreased as the replacement of MFA increased. The selected FA type manifested similar physical characteristics to OPC, except for the specific gravity. According to the product specifications, the specific surface area (fineness) of FA was identified as 365 m^2/kg, which is closer to the fineness of OPC (i.e., (330–340) m^2/kg). The specific gravity of FA was identified as 2.92, compared to 3.08 for OPC. The similarity in the fineness of FA and OPC proved to be insignificant on the cumulative bleeding of concrete. However, the small variation could be due to differences in the specific gravities of FA and OPC. It should also be noted that the cumulative bleeding of the C-series concrete was significantly lower than that of the P-series and M-series concrete at each replacement level, which could be due to the high range of water reduction in the mixes.

4.2 Effect of MFA on plastic shrinkage cracking severity

The severity of plastic shrinkage cracking could be correlated with the MFA replacements. The rate of bleeding of fresh concrete is a major factor in plastic shrinkage cracking [20–22]. The bleeding of concrete is influenced by the settlement rate of aggregate particles and the free-water content of the mix. Here, MS particles were 0.075 to 4.75 mm in size, while MFA particles were less than 0.075 mm. Therefore, the settlement rate of fine aggregate particles was quicker than that of the MFA particles due to the higher specific gravity.

Varying ranges of replacement with MFA enhanced different levels of plastic shrinkage cracking severity. As illustrated in Fig. 12, low, medium, and high severity levels ($w_1 < w_2 < w_3$) were achieved in concrete mixes with the selected replacement levels of MS by MFA. At smaller replacement levels, such as 0% and 3%, the bleeding was high due to the presence of larger MS particles, leading to low severity. This is because the reduced evaporation of the accumulated bleed water created low tensile stress in the concrete. When MS was replaced at higher levels, such as 9% and 12%, more smaller particles were introduced into the mix, reducing the amount of bleed water at the surface. As a result, the rapid evaporation caused higher tensile stress during concrete stiffening and led to high plastic shrinkage cracking severity.

4.3 Effect of MFA on crack initiation life

Crack initiation life was first measured for concrete specimens subjected to the plastic shrinkage cracking test. Figure 13 shows the effects of varying MFA on the crack initiation life of concrete. Similar trends were observed for both MS types, specifically, a decreasing trend was observed with increasing replacements by MFA. This could be due to the slower settlement rate of coarser particles at larger replacement levels by MFA as discussed under Subsection 4.2.

The C-series concrete mixes were first exposed to plastic shrinkage cracking where the crack initiation life of both MS types was less than 40 min at each MFA level due to the addition of SP, which highly reduced the water content in the mix. In the case of the M-series, the crack initiation life varied between 60 to 40 min as the replacement level increased from 0 to 12%. This resulted in a considerable increment in crack initiation life compared to the C-series due to an increased bleeding rate. The P-series concrete with 0% and 12% replacement with MFA exhibited a crack initiation life of 68 and 40 min, respectively, for MH concrete and 55 and 38 min, respectively, for MC concrete.

Based on the observations, a relationship can be modeled between the initiation life of plastic shrinkage cracking (t_i) and the cumulative bleeding of concrete (b), as illustrated in Fig. 14(a). Based on the best fitting trend

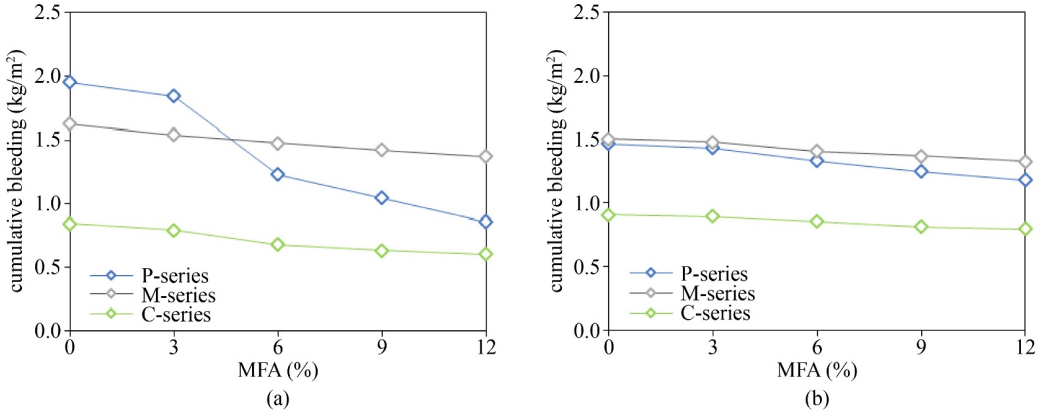

Fig. 11 Effect of MFA replacement levels on cumulative bleeding: (a) MC concrete; (b) MH concrete.

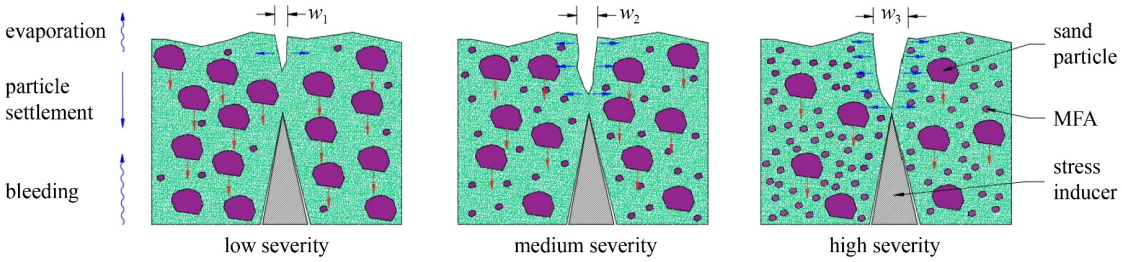

Fig. 12 Severity levels of plastic shrinkage cracking of concrete.

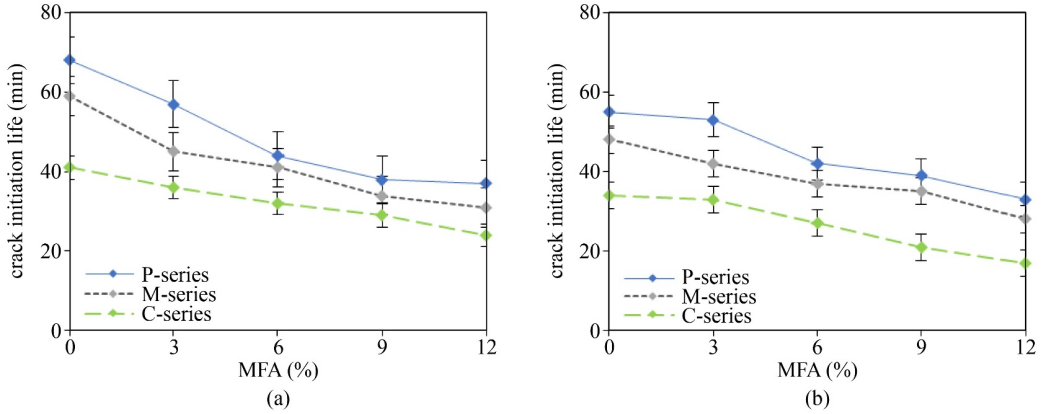

Fig. 13 Relationship between MFA content and crack initiation life: (a) MC concrete; (b) MH concrete.

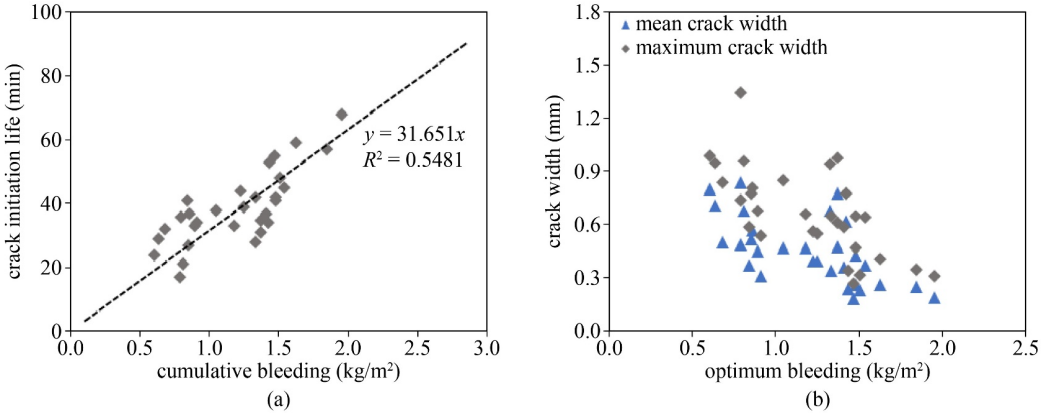

Fig. 14 (a) Crack initiation life vs cumulative bleeding; (b) crack width vs optimum bleeding.

line, a linear relationship, as provided in Eq. (1), was obtained with an *R*-squared value of 0.9643. As discussed above, an increasing crack initiation life trend was observed with the cumulative bleeding of concrete.

$$t_i = 31.651b. \quad (1)$$

4.4 Effect of MFA on crack profile

In general, cracks are classified based on their nature, dimensions, and shape [65,66]. However, this section focuses solely on the shape-wise classification to investigate the crack profiles. The experimental results were obtained from visual inspections and image processing, hence no quantitative analysis was carried out. Based on the 24-h observation of each mix, all specimens underwent the plastic shrinkage cracking test with the assigned environmental conditions. In certain specimens, both primary and secondary cracks were identified. However, only primary cracks were selected due to their dimensions and analysed to identify the crack profile.

The identification of crack profile was conducted as the fourth stage of the image processing model as shown in Fig. 6. Four different profiles of plastic shrinkage cracks were detected in this study. Figure 15 exhibits the processed images of the four crack types, specifically the continuous crack, segmented crack, branching crack, and

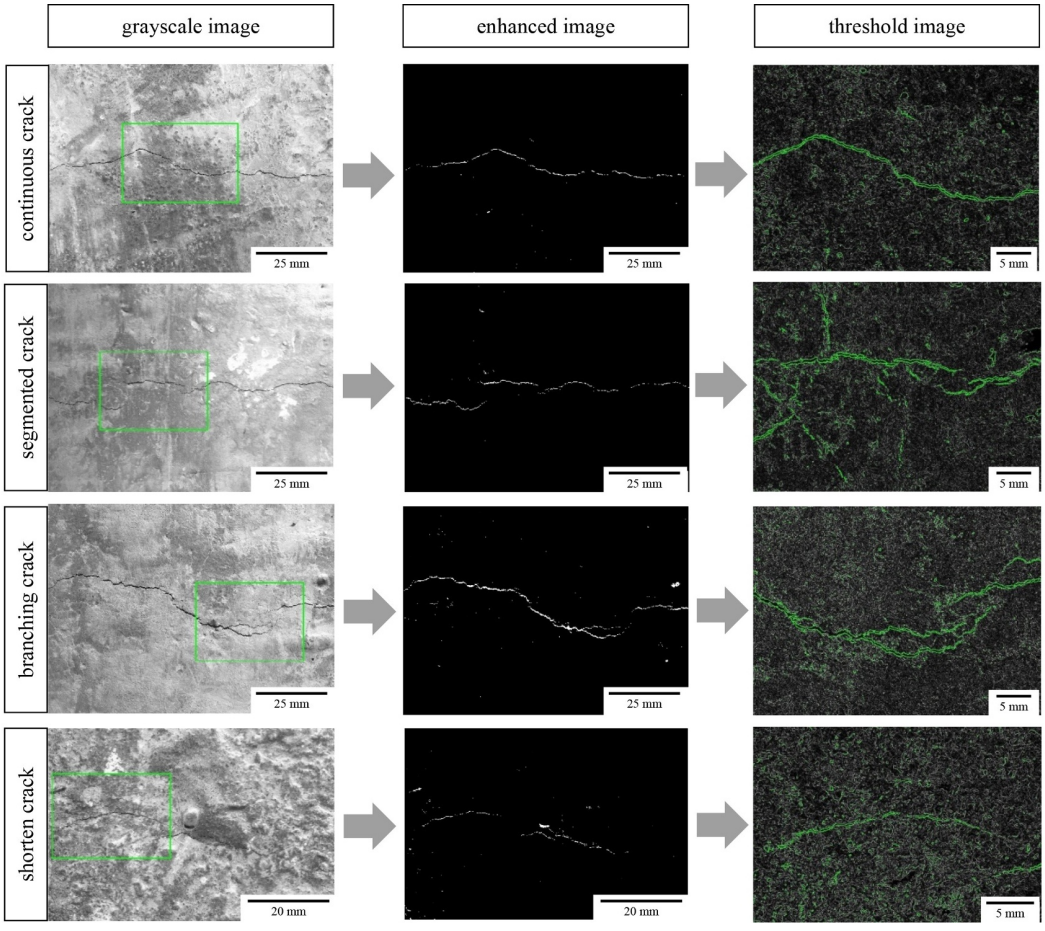

Fig. 15 ImageJ software processed images of typically identified crack patterns.

shortened crack. The following author-defined definitions of the four crack profiles mentioned above were used in this study to categorize the crack patterns observed in the specimens.

−Continuous crack: Crack initiated from or near one edge of the crack inducer and propagated to the other edge without any spacings or splits.

−Segmented crack: Crack initiated from or near one edge of the crack inducer and propagated to the other edge or ceased at an intermediate position with a combination of segments.

−Branching crack: Continuous or segmented crack diverged into branches at one or more locations along or near the profile of the crack inducer.

−Shortened crack: Crack initiated from any location along or near the profile of the crack inducer and propagated to a maximum length of 100 mm.

The grayscale, enhanced, and threshold images were obtained from image processing to analyze the crack profiles illustrated in Fig. 15. The grayscale images reveal the pictorial views of the actual concrete surface following calibration. The surface locations where the crack pattern and the author-defined cracks coincided were marked with squares, which were enlarged to produce the enhanced and threshold images. The enhanced images distinctly show the crack patterns after the modification of grayscale images. The threshold images provide additional visual evidence by clearly showing the enlarged views of the crack patterns detected from the grayscale images.

As discussed in Subsection 4.3, crack susceptibility increased as the MFA percentage increased. Based on the crack profiles, we can see that shortened and segmented cracks were detected at lower MFA levels, while continuous and branching cracks were observed at higher MFA levels. Shortened cracks were only formed when the concrete reached maximum bleeding at 0% replacement level. Based on Table 6, P-MH_0 and P-MH_3 were determined for shortened cracks.

Segmented cracks were detected when the concrete was exposed to medium susceptibility. The majority of the P-series, M-series, and C-series concrete with 3% and 6% replacement levels were failed by segmented cracks. This crack profile was, in general, shorter in length and width compared to that of the continuous and branching cracks. Due to the increase in MFA, bleeding was reduced and high tensile stress was created at the surface of concrete with 0% MFA. Segmented cracks formed when concrete was unable to dissipate the energy created by tensile stress through shortened cracks.

Table 6 Summary of crack features and measurements (values are in mm and mm^2)

mix	profile	width		depth		length	area
		mean	SD	mean	SD		
P-MC_0	segmented	0.19	0.062	11.15	1.45	96.85	18.35
P-MC_3	segmented	0.25	0.058	11.60	0.80	78.37	23.44
P-MC_6	segmented	0.40	0.095	9.80	1.40	174.24	79.68
P-MC_9	continuous	0.47	0.186	7.90	1.50	308.55	145.09
P-MC_{12}	branching	0.57	0.101	8.05	0.65	312.66	189.52
P-MH_0	shorten	0.18	0.060	13.90	0.30	115.84	19.85
P-MH_3	shorten	0.24	0.064	10.15	2.25	129.47	31.74
P-MH_6	continuous	0.34	0.170	9.90	0.50	295.24	105.32
P-MH_9	continuous	0.40	0.146	11.55	1.85	287.55	115.35
P-MH_{12}	segmented	0.47	0.120	12.22	3.26	320.61	155.79
M-MC_0	segmented	0.26	0.071	14.06	0.79	116.43	30.27
M-MC_3	segmented	0.37	0.127	11.53	1.72	154.28	53.14
M-MC_6	segmented	0.43	0.131	10.53	2.04	148.35	65.88
M-MC_9	branching	0.62	0.076	14.47	1.20	284.10	176.14
M-MC_{12}	continuous	0.78	0.188	15.02	3.38	311.25	242.84
M-MH_0	segmented	0.23	0.066	11.82	0.58	147.58	31.97
M-MH_3	segmented	0.26	0.102	16.90	2.54	177.89	46.82
M-MH_6	continuous	0.36	0.134	7.95	1.51	244.08	103.48
M-MH_9	continuous	0.48	0.109	14.36	0.59	308.98	148.31
M-MH_{12}	branching	0.68	0.169	13.40	1.26	305.84	201.46
C-MC_0	segmented	0.37	0.145	13.81	1.34	104.88	39.14
C-MC_3	segmented	0.49	0.141	6.66	2.82	115.37	56.53
C-MC_6	continuous	0.50	0.214	13.74	2.60	284.51	145.18
C-MC_9	branching	0.71	0.178	9.00	0.54	338.94	240.31
C-MC_{12}	branching	0.80	0.185	7.75	2.12	317.58	258.57
C-MH_0	segmented	0.31	0.107	10.72	0.31	100.73	31.62
C-MH_3	segmented	0.45	0.116	9.74	3.40	132.06	58.43
C-MH_6	segmented	0.52	0.157	5.75	0.59	189.34	98.47
C-MH_9	continuous	0.68	0.202	7.30	1.16	295.18	202.84
C-MH_{12}	branching	0.84	0.391	11.05	1.305	328.54	262.19

Note: SD represents the standard deviation of data.

Continuous and branching cracks propagated in concrete with higher MFA replacement levels, such as 9% and 12%, indicating high severity of plastic shrinkage cracking. Because of the lower concrete bleeding at high replacement levels, cracking was exacerbated due to the high tensile stress. However, bifurcations of cracks were created when concrete had inadequate capacity to dissipate the energy through a single continuous crack.

4.5 Effect of MFA on average and maximum crack widths

The average and maximum crack widths were the key parameters of the plastic shrinkage cracking test of concrete. The crack width should be carefully investigated since it is a major factor related to durability and structure failure. Figure 16 illustrates the effects of varying MFA levels in concrete on the average crack width. Based on the 24-h observations, the average crack width was determined for both MC and MH concretes for all replacement levels by MFA.

For the P-series, MC and MH concretes had average crack widths of 0.19 and 0.18 mm, respectively at 0% MFA content (see Table 6). However, the average crack widths at 12% MFA were 0.57 and 0.47 mm. Similar trends were observed for the M-series and C-series. The C-series concrete demonstrated the highest average crack

width for each selected replacement level by MFA, reflecting the significant impact of high range water reducers in concrete on the crack width. According to the values provided in Table 6, concrete that contained MH manifested crack widths slightly lower than that of MC concrete.

The maximum crack width of concrete also followed an increasing trend as the MFA content increased, as presented in Fig. 17. The P-series MC and MH concretes at 0% MFA content showed maximum crack widths of 0.32 and 0.30 mm, respectively, which later increased to 0.80 and 0.60 mm, respectively, at 12% replacement level of MS by MFA. The M-series and C-series MC concrete mixes showed slightly higher maximum crack widths than the P-series MC concrete. A similar behaviour could be identified for the MH concretes of each series.

Figure 14(b) is a graphic representation of the correlation between the average and maximum crack widths and concrete bleeding. Based on the data distribution, we can see that the average and maximum crack widths decreased as the optimum bleeding increased. The high tensile stress due to low bleeding resulted in the initiation and propagation of larger cracks (usually accompanied with larger widths) at the surfaces. We were unable to derive a direct relationship between the factors due to the low coefficient of determination values for the distribution of data.

4.6 Effect of MFA on crack length and crack area

The variations in crack length and crack area with respect to the replacement levels of MS by MFA are plotted in Fig. 18. A gradual increase in the crack length was observed as the MFA content in MC concrete increased from 3% to 6% and 3% to 9% in MH concrete (i.e., 78.37 to 174.24 mm for MC concrete and 129.47 to 295.24 mm for MH concrete). Due to the gradual increase in the crack widths and lengths, the crack area also increased as the replacement levels increased. As discussed previously, the actual crack area was measured using the image processing software in this study. The area encompassed by the purple boundary (see Fig. 7) represents the crack area measurement of a typical crack. This method could be more accurate than the traditional method of crack area calculation (multiplying the crack length by the average crack width). It was observed that the crack area of MC and MH concretes changed from 18.35 to 189.52 mm^2 and 19.85 to 155.79 mm^2, respectively, when the replacement level increased from 0% to 12%. The rationale behind these variations could be the lower

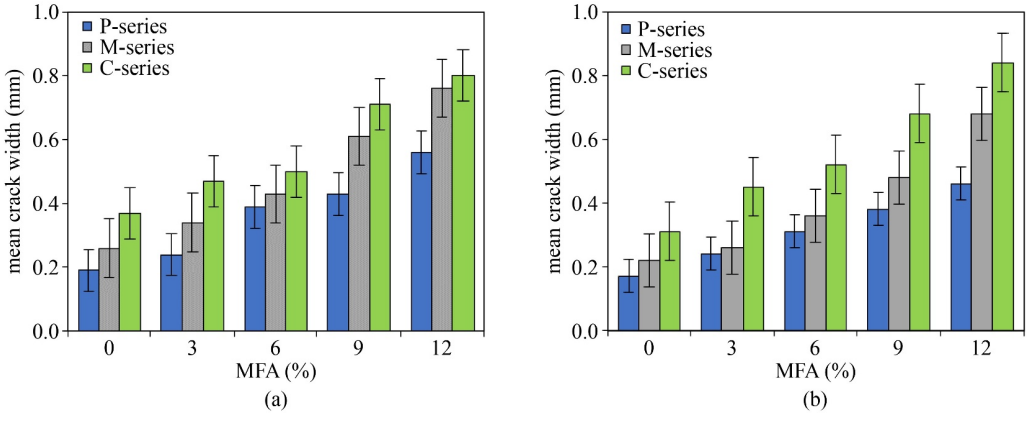

Fig. 16 Variation of mean crack width against MFA level: (a) MC concrete; (b) MH concrete.

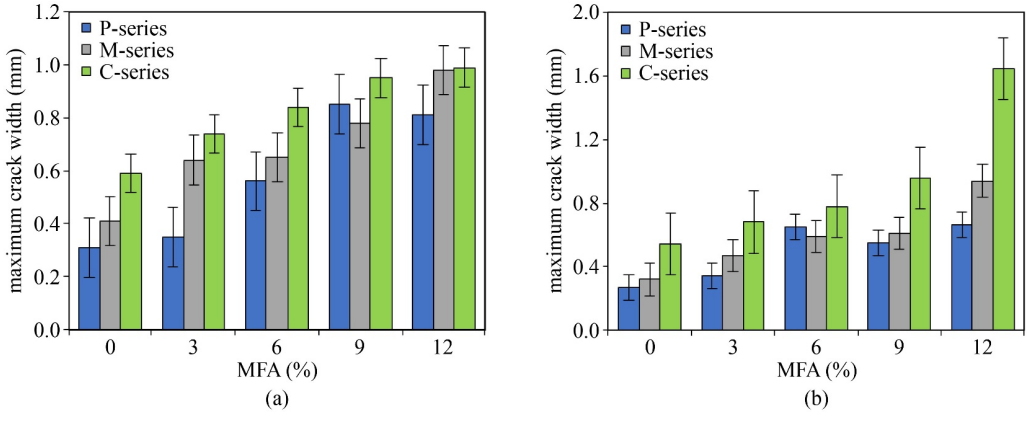

Fig. 17 Variation of maximum crack width against MFA level: (a) MC concrete; (b) MH concrete.

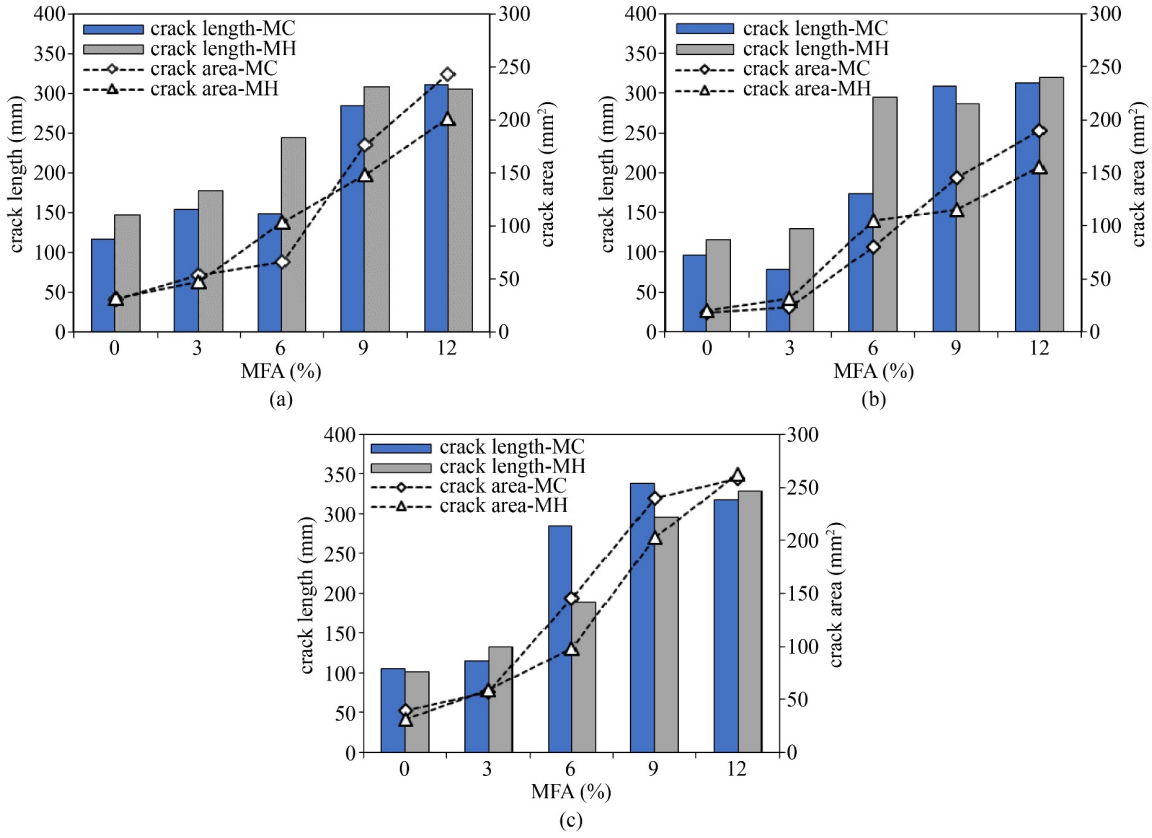

Fig. 18 Relationship of MFA content, crack length, and crack area: (a) P-series; (b) M-series; (c) C-series.

concrete bleeding at high MFA levels, resulting in increased crack length and crack area.

Concrete mixes that contained FA revealed a marginally higher crack length than that of the P-series concretes at smaller replacement levels. However, at high replacement levels, such as 9% and 12%, both MC and MH concretes demonstrated similar behaviours to the P-series concretes. The length of the MC and MH concrete cracks at 12% replacement were 63% and 52% higher than that of the MC_0 and MH_0 concretes at 0% replacement level. When the replacement level increased from 0% to 12%, the crack area also increased by 87% for MC concrete (from 30.27 to 242.84 mm^2) and 84% for MH concrete (from 31.97 to 201.46 mm^2).

The C-series concretes also revealed similar trends. Compared to the other series, the C-series exhibited remarkably higher crack lengths and crack areas. At 12% replacement level, the crack lengths of the C-series MC and MH concretes were 317.58 and 328.54 mm, respectively, which are 2% and 7% higher than their respective M-series concretes. At this replacement level, the crack area of C-series was measured as 258.57 mm^2 for MC concrete and 262.19 mm^2 for MH concrete, which are 6% and 23% greater than the M-series MC and MH concretes, respectively.

The above trends demonstrated by the M-series and C-series are attributable to the higher tensile stress created at the concrete surfaces as a result of the inclusion of admixtures. Both mineral and chemical admixtures selected for this study considerably reduced the water demand of the concrete mixes compared to the plain concrete, which led to an inability to resist tensile stress and shorter bleeding duration. This resulted in a significant increase in crack length and crack area compared to the P-series concretes.

4.7 Effect of MFA on crack depth

Crack depth was investigated based on visual observations and manual measurements using a micrometer, in other words, the image processing technique was not used for this analysis. The final crack depth was calculated as the average of the two depths observed at the longer spans of the specimen near to the stress riser. Table 6 shows the average crack depth of each concrete and their respective standard deviations. A distinct variation was not identified between the average crack depth and replacement levels of MS by MFA. Therefore, statistical analysis on the effects of MFA replacements on crack depth was not carried out.

The crack depth could vary along the profile of the stress inducer since the depth measurements were taken only on the longitudinal sides of concrete specimens, which may affect the accuracy of the average crack depth.

Thus, we are unable to draw accurate conclusions on the effects of MFA replacement levels on plastic shrinkage cracking depth. Future studies are necessary to evaluate the plastic shrinkage cracking depth at regular intervals along the profile of stress riser.

4.8 Level of statistical significance

Table 7 provides the *p*-values obtained from the single factor one-way *ANOVA* test for each concrete property mentioned in this study. Each *ANOVA* test was conducted with a degree of freedom of nine (9). The *p*-values were compared at a level of significance (α) of 0.05 (at 95% confidence interval) selected for this statistical analysis. Regarding the bleeding of concrete, results from the *ANOVA* test showed *p*-values of each concrete series between 0.708 and 0.787. This range is higher than the level of significance, thus can be concluded that the replacement levels with MFA has no statistically significant effect on the bleeding of concrete. Since the *p*-values of crack initiation life of concrete were between 0.996 and 1.000, we can also conclude that the varying MFA levels has no significant impact on crack initiation life.

The average and maximum crack width, crack length (*p*-values between 0.864–0.975), and crack area (*p*-values between 0.699–0.799) measurements also showed no statistical significance for the selected MFA replacement levels since the *p*-values were above the significance level. Hence, it can be concluded that the replacement levels of MS with MFA did not have a significant impact on the bleeding and plastic shrinkage cracking properties of concrete.

5 Conclusions

The effects of varying replacement levels of MS by MFA, from 0% to 12% at 3% increments by weight, on the bleeding and vulnerability to plastic shrinkage cracking of concrete were investigated in this study. The combined influence of mineral and chemical admixtures and the replacement levels were reported. The major conclusions derived from the experiment results are as followed.

1) The increasing replacement levels by MFA declined the rate of concrete bleeding. A gradual increase followed by a less gradual trend was observed for each replacement level. The cumulative bleeding of concrete uniformly decreased with the increasing MFA substitutions. The main factors that influence the rate of bleeding were determined as the replacement of larger particles by MFA and the varying water demand with the addition of mineral and chemical admixtures.

2) The susceptibility to plastic shrinkage cracking of concrete was evaluated based on the crack features obtained from an image processing technique. Three severity models of plastic shrinkage cracking were proposed in this study, specifically low severity, medium severity, and high severity according to the crack measurements. In addition, these severity models were verified with the initiation life of plastic shrinkage cracks.

3) The crack initiation life decreased as the MFA contents in concrete increased and the rate of declination increased in the order of C-series < M-series < P-series. The rationale behind this is the evaporation of accumulated water at the concrete surface was accelerated by the low bleeding rates at higher replacement levels by MFA. After the complete propagation of cracks in each specimen, four patterns were detected, specifically the continuous crack, segmented crack, branching crack, and shorten crack.

4) The experimental results clearly show that the average and maximum crack widths increased as the replacement level increased from 0% to 12%. The highest average and maximum crack widths were detected for the C-series concrete, followed by the M-series and P-series concretes. An inverse relationship was identified between the crack widths and cumulative bleeding of concrete. On the other hand, a positive correlation was observed between the crack length/area and the increasing replacement levels due to the high tensile stress caused by early evaporation at higher replacements of MS with MFA (i.e., 9% and 12%).

5) Finally, the severity of plastic shrinkage cracking of

Table 7 *p*-values of single factor one-way *ANOVA* test

property	P-series		M-series		C-series	
	MC concrete	MH concrete	MC concrete	MH concrete	MC concrete	MH concrete
bleeding	0.787 (0.424)	0.724 (0.525)	0.708 (0.551)	0.708 (0.552)	0.761 (0.463)	0.745 (0.490)
crack initiation life	0.996 (0.038)	0.999 (0.014)	0.997 (0.029)	1.000 (0.007)	1.000 (0.004)	1.000 (0.016)
mean crack width	0.745 (0.491)	0.733 (0.509)	0.727 (0.520)	0.716 (0.539)	0.725 (0.524)	0.654 (0.646)
maximum crack width	0.713 (0.543)	0.733 (0.509)	0.710 (0.548)	0.716 (0.539)	0.708 (0.551)	0.654 (0.646)
crack length	0.864 (0.305)	0.936 (0.185)	0.932 (0.194)	0.975 (0.106)	0.917 (0.228)	0.914 (0.224)
crack area	0.699 (0.566)	0.768 (0.454)	0.726 (0.522)	0.791 (0.417)	0.799 (0.406)	0.759 (0.469)

Note: Values in parenthesis represent the *F*-values.

concrete was advanced (from low severity to high severity) with the increasing replacements of MS with MFA (i.e., from 0% to 12%). Results from the statistical analysis showed that the selected replacements did not have significant effects on the bleeding and plastic shrinkage properties of MC and MH concretes at 95% confidence interval.

Acknowledgements The authors are grateful to INSEE Siam City, Sri Lanka for providing the necessary binding materials to conduct this study. Furthermore, the authors wish to thank all technical staffs of the Department of Civil Engineering, University of Sri Jayewardenepura for their support on the experimental work.

References

1. He H, Wang Y, Wang J. Effects of Aggregate micro fines (AMF), aluminium sulfate and polypropylene fiber (PPF) on properties of machine-made sand concrete. Applied Sciences (Basel, Switzerland), 2019, 9(11): 2250
2. Branavan A, Konthesingha K M C. Fine aggregate usage in concrete and masonry mortar by local construction industries. In: Proceedings of 10th International Conference on Structural Engineering and Construction Management (ICSECM). Kandy: Nethwin printers, 2019, 106−113
3. Gavriletea M D. Environmental impacts of sand exploitation. Analysis of sand market. Sustainability (Basel), 2017, 9(7): 1118
4. Cortes D D, Kim H K, Palomino A M, Santamarina J C. Rheological and mechanical properties of mortars prepared with natural and manufactured sands. Cement and Concrete Research, 2008, 38(10): 1142−1147
5. Ding X, Li C, Xu Y, Li F, Zhao S. Experimental study on long-term compressive strength of concrete with manufactured sand. Construction & Building Materials, 2016, 108: 67−73
6. Arulmoly B, Konthesingha C, Nanayakkara A. Performance evaluation of cement mortar produced with manufactured sand and offshore sand as alternatives for river sand. Construction & Building Materials, 2021, 297(7): 123784
7. Arulmoly B, Konthesingha C, Nanayakkara A. Effects of blending manufactured sand and offshore sand on rheological, mechanical, and durability characterization of lime-cement masonry mortar. European Journal of Environmental and Civil Engineering, 2021, 1−27
8. Li L, Wang B, Hubler M H. Carbon nanofibers (CNFs) dispersed in ultra-high performance concrete (UHPC): Mechanical property, workability and permeability investigation. Cement and Concrete Composites, 2022, 131: 104592
9. Abbas S, Nehdi M L, Saleem M A. Ultra-high performance concrete: Mechanical performance, durability, sustainability and implementation challenges. International Journal of Concrete Structures and Materials, 2016, 10(3): 271−295
10. Meng W, Khayat K G. Mechanical properties of ultra-high performance concrete enhanced with granite nanoplatelets and carbon nanofibers. Composites. Part B, Engineering, 2016, 107: 113−122
11. Arulmoly B, Konthesingha C, Nanayakkara A. Influence of mortars comprised of manufactured sand with offshore sand on the performance of masonry and brick–mortar joint. Innovative Infrastructure Solutions, 2022, 7(2): 160
12. Arulmoly B, Konthesingha C, Nanayakkara A. Influence of blended fine aggregates on the performance of lime-cement mortar—A statistical approach. In: Proceedings of 7th International Multidisciplinary Engineering Research Conference (MERCon 2021). Colombo: IEEE Xplore, 2021
13. Li B, Wang J, Zhou M. Effect of limestone fines content in manufactured sand on durability of low- and high-strength concretes. Construction & Building Materials, 2009, 23(8): 2846−2850
14. Wang J, Niu K, Tian B, Sun L. Effect of methylene blue (MB)-value of manufactured sand on the durability of concretes. Journal of Wuhan University of Technology—Material Science Edition, 2012, 27(6): 1160−1164
15. Li C. Effects of micro fines content on workability and mechanical properties of manufactured sand concrete. In: 2016 International Conference on Material Science and Civil Engineering (MSCE 2016). Guangzhou: MSCE, 2017
16. Stewart J, Novell J, Juenger M, Fowler D W. Characterizing minus No. 200 Fine Aggregate for Performance in Concrete. ICAR Technical Reports ICAR-107-1. 2006
17. Gotmare P G, Sheth A J. Influence of fines and microfines on properties of concrete. International Journal of Engineering Research in Mechanical and Civil Engineering, 2017, 2(4): 38−41
18. Hashemi M, Shafigh P, Abbasi M, Asadi I. The effect of using low fines content sand on the fresh and hardened properties of roller-compacted concrete pavement. Case Studies in Construction Materials, 2019, 11: 1−11
19. Boshoff W P, Combrinck R. Modelling the severity of plastic shrinkage cracking in concrete. Cement and Concrete Research, 2013, 48: 34−39
20. Sayahi F, Emborg M, Hedlund H, Cwirzen A, Stelmarczyk M. The severity of plastic shrinkage cracking in concrete: a new model. Magazine of Concrete Research, 2021, 73(6): 315−324
21. Radocea A. A model of plastic shrinkage. Magazine of Concrete Research, 1994, 46(167): 125−132
22. Uno P J. Plastic shrinkage cracking and evaporation formulas. ACI Materials Journal, 1998, 95(4): 365−375
23. Ghourchian S, Wyrzykowski M, Baquerizo L, Lura P. Susceptibility of Portland cement and blended cement concretes to plastic shrinkage cracking. Cement and Concrete Composites, 2018, 85: 44−55
24. Yang K, Zhong M, Magee B, Yang C, Wang C, Zhu X, Zhang Z. Investigation of effects of Portland cement fineness and alkali content on concrete plastic shrinkage cracking. Construction & Building Materials, 2017, 144: 279−290
25. Matalkah F, Jaradat Y, Soroushian P. Plastic shrinkage cracking and bleeding of concrete prepared with alkali activated cement. Heliyon, 2019, 5(4): e01514
26. Rahmani T, Kiani B, Bakhshi M, Shekarchizadeh M. Application of different fibers to reduce plastic shrinkage cracking of concrete. In: 7th RILEM International Conference on Cracking in Pavements. Delft: RILEM, 2012, 635−642

27. Banthia N, Gupta R. Influence of polypropylene fiber geometry on plastic shrinkage cracking in concrete. Cement and Concrete Research, 2006, 36(7): 1263−1267
28. Branch J, Rawling A, Hannant D J, Mulheron M. The effects of fibers on the plastic shrinkage cracking of high strength concrete. Materials and Structures, 2002, 35(3): 189−194
29. Nam J, Kim G, Yoo J, Choe G, Kim H, Choi H, Kim Y. Effectiveness of fiber reinforcement on the mechanical properties and shrinkage cracking of recycled fine aggregate concrete. Materials (Basel), 2016, 9(3): 131
30. Arya E K, James J S, John E. Study on the effectiveness of shrinkage reducing admixtures on plastic shrinkage of concrete. In: Proceedings of SECON'19. Angamaly: Springer, 2020
31. Sirajuddin M, Gettu R. Plastic shrinkage cracking of concrete incorporating mineral admixtures and its mitigation. Materials and Structures, 2018, 51(2): 48
32. Kosmatka S H, Panarese W C, Kerkhoff B. Design and Control of Concrete Mixtures. Skokie, IL: Portland Cement Association, 2002, 79−103
33. Branavan A, Konthesingha K M C, Nanayakkara S M A, Premasiri H M R. Optimizing blending of manufactured sand with offshore sand based on physical and virtue characteristics. Journal of Materials Science Research and Reviews, 2020, 6(3): 11−31
34. Dias W P S. Influence of mix and environment on plastic shrinkage cracking. Magazine of Concrete Research, 2003, 55(4): 385−394
35. Sivakumar A. Studies on influence of water−cement ratio on the early age shrinkage cracking of concrete systems. Journal of Civil Engineering and Construction Technology, 2013, 4(1): 1−5
36. Sun D, Shi H, Wu K, Miramini S, Li B, Zhang L. Influence of aggregate surface treatment on corrosion resistance of cement composite under chloride attack. Construction & Building Materials, 2020, 248: 118636
37. Sun D, Huang C, Cao Z, Wu K, Zhang L. Reliability assessment of concrete under external sulfate attack. Case Studies in Construction Materials, 2021, 15: e00690
38. Chen S, Duffield C, Miramini S, Nasim Khan Raja B, Zhang L. Life-cycle modelling of concrete cracking and reinforcement corrosion in concrete bridges: A case study. Engineering Structures, 2021, 237: 112143
39. BS 882:1992. Specification for Aggregates from Natural Sources for Concrete. London: BSI, 1992
40. EN 197-1:2000. Cement—Part 1: Composition, Specifications and Conformity Criteria for Common Cements. London: BSI, 2000
41. ASTM C33/C33M-18. Standard Specification for Concrete Aggregates. West Conshohocken, PA: ASTM International, 2018
42. Shen W, Yang Z, Cao L, Cao L, Liu Y, Yang H, Lu Z, Bai J. Characterization of manufactured sand: Particle shape, surface texture and behaviour in concrete. Construction & Building Materials, 2016, 114: 595−601
43. ASTM C294-19. Standard Descriptive Nomenclature for Constituents of Concrete Aggregates. West Conshohocken, PA: ASTM International, 2019
44. ASTM C144-03. Standard Specification for Aggregate for Masonry Mortar. West Conshohocken, PA: ASTM International, 2003
45. ASTM C128-01. Standard Test Method for Density, Relative Density (Specific Gravity) and Absorption of Fine Aggregate. West Conshohocken, PA: ASTM International, 2001
46. ASTM C1252-03. Standard Test Methods for Uncompacted Void Content of Fine Aggregate (as Influenced by Particle Shape, Surface Texture, and Grading). West Conshohocken, PA: ASTM International, 2003
47. ASTM C29/C29M-97. Standard Test Method for Bulk Density ("Unit Weight") and Voids in Aggregate. West Conshohocken, PA: ASTM International, 1997
48. ASTM C70-06. Standard Test Method for Surface Moisture in Fine Aggregate. West Conshohocken, PA: ASTM International, 2006
49. ASTM C117-95. Standard Test Method for Materials Finer than 75-μm (No. 200) Sieve in Mineral Aggregates by Washing. West Conshohocken, PA: ASTM International, 1995
50. ASTM D7928-17. Standard Test Method for Particle-Size Distribution (Gradation) of Fine-Grained Soils Using the Sedimentation (Hydrometer) Analysis. West Conshohocken, PA: ASTM International, 2017
51. Sandberg M E, Sandberg S V. Investigating the causes of deterioration in concrete blocks in Southern Ireland. In: 17th Euroseminar on Microscopy Applied to Building Materials (EMABM). Toronto: University of Toronto, 2019
52. Johansson E, Miskovsky K, Loorents K J, Löfgren O. A method for estimation of free mica particles in aggregate fine fraction by image analysis of grain mounts. Journal of Materials Engineering and Performance, 2008, 17(2): 250−253
53. Osorio J P. What is mica and why it is important for Irish homeowners? 2021 (Available at the website of RTÉ)
54. ASTM C618-19. Standard Specification for Coal Fly Ash and Raw or Calcined Natural Pozzolan for Use in Concrete. West Conshohocken, PA: ASTM International, 2019
55. ASTM C494/C494M-19. Standard Specification for Chemical Admixtures for Concrete. West Conshohocken, PA: ASTM International, 2019
56. BS 812:1995. Testing Aggregates—Part 2: Methods of Determination of Density. London: BSI, 1995
57. ASTM C143/C143M-20. Standard Test Method for Slump of Hydraulic-Cement Concrete. West Conshohocken, PA: ASTM International, 2020
58. ASTM C232/C232M-20. Standard Test Method for Bleeding of Concrete. West Conshohocken, PA: ASTM International, 2020
59. ASTM C1579-13. Standard Test Method for Evaluating Plastic Shrinkage Cracking of Restrained Fiber Reinforced Concrete (Using a Steel Form Insert). West Conshohocken, PA: ASTM International, 2013
60. Sayahi F. Plastic shrinkage cracking in concrete: Mitigation and modelling. Dissertation for the Doctoral Degree. Norrbotten County: Lulea University of Technology, 2019
61. Sivakumar A, Santhanam M. Measuring, Monitoring and Modeling Concrete Properties. Dordrecht: Springer, 2006, 291−296
62. Arulmoly B, Konthesingha C, Nanayakkara A. Plastic settlement and hardened state assessments of manufactured sand made concrete for varying microfine levels. Structural Concrete, 2022,

1−21
63. Qi C, Weiss J, Olek J. Characterization of plastic shrinkage crackig in fiber reinforced concrete using image analysis and a modified Weibull function. Materials and Structures, 2003, 36(6): 386−395
64. Turkmenoglu H N, Atahan H N, Sengul C. The use of polypropylene fibers against plastic shrinkage cracking. Proceedings of International Structural Engineering and Construction, 2016, 3(1): 23−28
65. Nandakishore P, Goehring L. Crack patterns over uneven substrates. Soft Matter, 2016, 12(8): 2253−2263
66. Thulasi T K, Subathra S, Meikandaan T P. An experimental study of crack patterns on reinforced concrete beam. International Research Journal of Engineering and Technology, 2018, 5(3): 3195−3202